minerals

MDPI

Article

Microstructure Evaluation of Fly Ash Geopolymers Alkali-Activated by Binary Composite Activators

Jiangping Zhao and Yachao Wang *

School of Resources Engineering, Xi'an University of Architecture & Technology, Xi'an 710055, China; zhaojiangping@xauat.edu.cn

* Correspondence: wangyachao@xauat.edu.cn

Abstract: An efficient fabrication of fly-ash-based geopolymer is urgent and necessary to develop solid waste recycling techniques. Herein, an attempt to investigate the effect of binary composite activators on the microstructure of fly-ash-based geopolymers is conducted through the comparison of 24 experiments, which consisted of $Na_2SiO_3 \cdot 9H_2O$, Na_2CO_3, K_2CO_3, NaOH, and KOH through a facile preparation technique. The results demonstrate that the activator of $Na_2SiO_3 \cdot 9H_2O$ + KOH presents the highest mechanical strength, due to the synergy activation between the inherent ≡Si-O-Si≡ silicon-chain precursor derived from the Na_2SiO_3 and K^+'s catalysis. It reveals that the K^+ plays a crucial role in the Na_2SiO_3-activated fly ash geopolymer, which is the rate-determining step of the enhanced crosslinking and propagation of N-(C)-A-S-H chains, leading to an increase in weight loss temperatures of specimens from TG/DTG results. Furthermore, the adding silica fume facilitates as-formed amorphous silicates, which also could fill into the pores of N-(C)-A-S-H amorphous gels and present a uniform and compact morphology, leading to an increase in the pore volume of the pore diameter less than 100 nm. It explores an efficient and cost-effective preparation of fly-ash-based geopolymer for developing solid waste recycling techniques.

Keywords: alkali-activated; microstructure; fly ash; binary activator; crosslinking

check for updates

Citation: Zhao, J.; Wang, Y. Microstructure Evaluation of Fly Ash Geopolymers Alkali-Activated by Binary Composite Activators. *Minerals* **2023**, *13*, 910. https://doi.org/10.3390/min13070910

Academic Editor: Alexander Mikhailovich Kalinkin

Received: 30 May 2023
Revised: 3 July 2023
Accepted: 3 July 2023
Published: 5 July 2023

Copyright: © 2023 by the authors. Licensee MDPI, Basel, Switzerland. This article is an open access article distributed under the terms and conditions of the Creative Commons Attribution (CC BY) license (https://creativecommons.org/licenses/by/4.0/).

1. Introduction

The mechanisms governing the formation of alkali-activated fly-ash-based geopolymer have been an area of intense investigation [1,2]; as an alternative to traditional Portland cement, one of the fundamental assumptions in the study of geopolymer formation has been that soluble alumina and silica undergo a dissolution–reorientation–solidification process to form geopolymeric materials, and further studies are still critical for its pervasive application [3–5]. According to the reports of journal literature on fly-ash-based geopolymer [6,7], activated by phosphoric acid and alkaline activators such as Na_2SiO_3, NaOH, K_2SiO_3, and KOH, cementitious material serves as a replacement for ordinary cement. Generally, an efficient and cost-effective fabrication of fly-ash-based geopolymer is urgent and necessary to develop solid waste recycling techniques.

Currently, the exploration and research on the binary composite activators have been important issues, in order to obtain excellent usability and low preparation cost. Binary activators consist of two kinds of different activators to generate synergetic activation, which facilitates a co-activation system. Komljenovic et al. [8] used aqueous solutions of $Ca(OH)_2$, NaOH, NaOH + Na_2CO_3, KOH, and sodium silicate (water glass) of various concentrations as alkali-activators, and proposed that the high strength was directly related to the high Si/Al ratio; the greater the Si/Al ratio in the reaction products, the higher the strength. Moreover, the activation potential of the activators investigated (taking equal concentrations into account) could be represented by the following: KOH < NaOH + Na_2CO_3 < NaOH < $Na_2O \cdot nSiO_2$. Cheng et al. [9] found that with the increasing K_2O content, the setting time increased, the compressive strength raised, and the fire resistance

characteristics were also improved in slag-based geopolymers. It was found that calcium ions did not simply balance the charge, but also acted as structural links to maintain the connectivity of the geopolymer network, inducing a more condensed structure as long polysialate chains suggest high cross-linking geopolymerical frameworks [10]. The $Ca(OH)_2$ mixing with K_2CO_3 as an alkaline activator solution was used to prepare a kaolin-based geopolymer [11]. Wang et al. [12] investigated the effect of the alkali admixture, activator modulus, and water–binder ratio on the workability, rheology, and geopolymerization of the fly ash geopolymer activated by the composite of sodium hydroxide and sodium silicate. Similarly, the carbonate and potassium have been explored for geopolymerical preparation, but there is less literature to conduct a comparative study on the micro-structures of fly-ash-based geopolymer activated by the single KOH, NaOH, Na_2CO_3, K_2CO_3, Na_2SiO_3, and their binary composites.

Furthermore, the composite activators consisting of solid waste have been gaining increased attention, and include calcium carbide residue and Glauber's salt [13], calcium carbide slag and sodium metasilicate powder [14], and salt-loss soda residue and oxalic acid [15]. Essentially, the alkali-activation is the chemical interaction between cations such as K^+, Na^+, and Ca^{2+}, and anions such as CO_3^{2-}, OH^-, SiO_3^{2-}, and PO_4^{3-}; the depolymerized silica tetrahedra are prone to crosslinking the activated aluminum-oxygen tetrahedra or octahedral and transforming into N-(C)-A-S-H chains or networks [14,15], and the cations are trapped into the networks for an equilibrium charge. However, different ions could facilitate or inhibit the crosslinking or grafting reactions among the N-(C)-A-S-H chains involved in the geopolymers, altering the route for reactive silicates $Si(OH)_4$ and aluminates $[Al(OH)_4]^-$ in fly ash, depolymerizing and restructuring into N-(C)-A-S-H amorphous gels. The as-formed cross-linking network structures exert excellent mechanical strength and duration theoretically, corresponding to a strong activation.

However, regarding the fly-ash-based geopolymer, the previous research has failed to consider the synergy between K^+ and SiO_3^{2-}, on the way to deepening the geopolymerical mechanisms. It preliminarily focuses on the synergetic effects of cations such as K^+ and Na^+, and anions such as CO_3^{2-}, OH^-, and SiO_3^{2-} in this article. A series of comparative studies on the micro-structures and mechanical performance of fly-ash-based geopolymer is conducted systematically, and is activated by various alkaline binary activators with different concentrations including $Na_2SiO_3{\cdot}9H_2O$, Na_2CO_3, K_2CO_3, NaOH, and KOH, respectively. The techniques are employed to clarify the micro-structure of different samples, including the testing of mechanical strength, scanning electron microscope (SEM), mercury intrusion porosimetry (MIP), thermogravimetry/differential thermogravimetry (TG/DTG), and X-ray diffraction (XRD). The novelty lies in pursuing the optimum formulation of the alkaline binary composite activator for preparing the fly-ash-based geopolymer, elucidating the corresponding mechanism among the various binary activators to prepare the geopolymer with an effective-cost performance. It favors the development of a circular ecological economy, prompting the green and cleaner techniques of cementitious composites.

2. Materials and Characterization

2.1. Starting Materials and Preparation of Specimens

Fly ash was obtained from the Hancheng power plant in Xi'an of China and ground to the Blaine specific surface area of 560 m^2/kg with a density of 2.45 g/cm^3; its average particle diameter equaled 11.8 μm, which was tested by a laser particle size analyzer, and the chemical composition was measured by X-ray fluorescence (XRF), as shown in Table 1. SF was collected from Linyuan company with a Blaine specific surface area of 25 m^2/g and a mean particle size of 2.6 μm, as well as 86 wt% SiO_2. Alkali-activators, including $Na_2SiO_3{\cdot}9H_2O$, Na_2CO_3, K_2CO_3, NaOH, and KOH, were purchased from Xi'an chemical reagent company of China; they belonged to the grade of an analytical reagent.

Table 1. Chemical composition of fly ash (wt%).

Composition	SiO_2	Al_2O_3	Fe_2O_3	CaO	K_2O	SO_3	TiO_2	Loss
Weight percent	50.16	36.25	4.46	3.85	1.84	0.54	1.18	1.76

2.2. Preparation of Specimens

The $Na_2SiO_3 \cdot 9H_2O$ (15 wt%), Na_2CO_3 (1 mol/L, 2 mol/L), K_2CO_3 (1 mol/L, 2 mol/L), NaOH (4 mol/L, 8 mol/L), KOH (4 mol/L, 8 mol/L) and their binary composite solutions were employed as alkali-activators, as shown in Table 2, respectively. The fly-ash-based geopolymerical pastes were prepared by stirring a mixture of fly ash and activator solution with a water/FA ratio of 0.30 to form the slurry, according to the standard of JC/T 729-2005 for testing the mechanical property of cement paste, which was stirred in the cement mortar machine of the SJ-160 type. Then, the slurry was poured into the stainless triplet mold of $50 \times 32.5 \times 32.5$ mm^3 with 1 min of vibrating on the vibrating table of ZT-96 type, and demoulded after curing for 9 h at an elevated temperature of 85 °C in the oven. Finally, specimens were cured for another 27 days in a curing chamber at room temperature with 90% humidity to evaluate their performances. Because the specimen is too small to test its flexural strength, only the compressive strength is provided in this paper.

Table 2. Compressive strength of specimens with different alkali-activators.

Sample	Activator Composition					Compressive Strength (MPa)		
	$Na_2SiO_3 \cdot 9H_2O$	Na_2CO_3	K_2CO_3	NaOH	KOH	3 d	7 d	28 d
S1	15 wt%	0	0	0	0	19.83	20.08	20.25
S2	0	1 mol/L	0	0	0	1.50	1.58	1.75
S3	0	2 mol/L	0	0	0	2.00	2.42	5.25
S4	0	0	1 mol/L	0	0	0.08	0.17	0.17
S5	0	0	2 mol/L	0	0	0.17	0.17	0.25
S6	0	0	0	4 mol/L	0	4.83	5.25	6.42
S7	0	0	0	8 mol/L	0	21.33	23.00	15.67
S8	0	0	0	0	4 mol/L	2.08	2.17	2.30
S9	0	0	0	0	8 mol/L	15.92	11.83	10.80
S10	0	0	0	4 mol/L	4 mol/L	8.75	10.83	9.58
S11	0	0	0	8 mol/L	4 mol/L	21.83	33.25	30.92
S12	15 wt%	1 mol/L	0	0	0	29.1	31.25	32.50
S13	15 wt%	2 mol/L	0	0	0	30.67	33.08	35.50
S14	15 wt%	0	1 mol/L	0	0	33.67	34.82	39.17
S15	15 wt%	0	2 mol/L	0	0	38.08	40.25	43.08
S16	15 wt%	0	0	4 mol/L	0	9.63	10.42	10.67
S17	15 wt%	0	0	0	4 mol/L	54.08	54.67	56.08
S18	15 wt%	0	0	0	8 mol/L	51.71	53.93	55.17
S19	0	1 mol/L	0	4 mol/L	0	17.50	17.92	18.25
S20	0	2 mol/L	0	4 mol/L	0	20.17	21.08	21.92
S21	0	0	1 mol/L	0	4 mol/L	4.92	4.92	5.17
S22	0	0	2 mol/L	0	4 mol/L	4.25	4.50	4.68
S23	0	2 mol/L	2 mol/L	0	0	0.17	0.17	0.25
S24	0	2 mol/L	0	0	4 mol/L	5.25	5.42	5.50

To further understand the effects of different ions during the process of geopolymerization, silica fume (SF) as a supplier of activated Si units was applied to preparing the specimen by mixing 10 wt% SF with 90 wt% fly ash as starting materials. The S25~S27 corresponds to the samples of fly ash/SF (fly ash: SF = 90:10, wt%) geopolymer, which was activated by 15% Na_2SiO_3, 15% Na_2SiO_3 + 4 M KOH, and 15% Na_2SiO_3 + 2 M K_2CO_3, respectively.

2.3. Characterizations

Compressive strengths were tested by a full-automatic cement compressive testing machine of YAW-300 type with a pressurization rate of 2.4 kN/s. The strength was obtained from the average value of three samples with a standard deviation under 10%. The morphology analysis was conducted on a Quanta 200 scanning electron microscope (SEM) with a working voltage of 20 kV and a vacuum degree of 10^{-5} torr. The fracture surface of samples was sprayed gold prior for scanning with an area of about 0.7~1.1 cm^2. The thermogravimetric (TG) analysis of Mettler measured the real-time weight loss of specimens during the heating process of 50–950 °C under a nitrogen atmosphere at a heating rate of 30 °C/min, and the DTG was obtained by the differential weight during heating. Pore size distributions of samples were measured by AUTOPORE 9500 mercury intrusion porosimetry (MIP) under a nitrogen pressure of 0.3 MPa. X-ray diffraction (XRD) patterns of specimens were measured on a D/MAX-2400 X-ray diffractometer equipped with a rotation anode using Cu Kα radiation, and the operating voltage and current were 40 kV and 40 mA, respectively. The sample was ground into powder to be filled in the slide grooves for X-ray diffraction.

3. Results

3.1. Mechanical Properties

The compressive strength of all the specimens with different alkali activators is shown in Table 2, which is obtained from the average value of three replicates as the final result with a standard deviation <10%. It is noted that all specimens exhibit an increase in the compressive strength from the aging of 3 d to 28 d, respectively, indicating that the geopolymerization involved in various systems has not completely reacted after a heat curing of 85 °C for 9 h. The single K^+-based activators exhibit weaker activation efficiency than Na^+, considering the strength as the reference.

The highest compressive strength presents on specimen S17 with binary composite activators of 15 wt% $Na_2SiO_3 \cdot 9H_2O$ + 4 mol/L KOH; it becomes 56.08 MPa at an aging of 28 d. It is in agreement with the Juho that the use of potassium silicate rather than sodium aluminate as an activator results in higher strength [16]. However, the excess NaOH is harmful to the mechanical strength, leading to a decrease in the compressive strength. Gökhan et al. [17] found that the optimal thermal curing temperature and the optimal NaOH concentration were 85 °C and 6 M, respectively.

Assuming the use of compressive strength as an evaluation criterion of the activation efficiency, which is directly related to mechanical strength, the following can be identified as (taking into account the equal concentration of cations): (1) for K^+, K_2CO_3 < K_2CO_3 + KOH < KOH; (2) for Na^+, Na_2CO_3 < Na_2CO_3 + KOH < Na_2CO_3 + NaOH < NaOH; (3) for the binary mixture, Na_2SiO_3 + NaOH < Na_2SiO_3 + Na_2CO_3 < Na_2SiO_3 + K_2CO_3 < Na_2SiO_3 + KOH, respectively.

However, excess OH^- holds an adverse effect; to the disadvantage of the compressive strength, the strength (10.67 MPa) of specimen S16 with activated Na_2SiO_3 + NaOH is inferior to the specimen (S1, 20.25 MPa) with Na_2SiO_3 activated only. It is in agreement with the report of Kiatsuda et al. [18] that a critical OH^- is crucial to attaining a specimen with excellent mechanical performance. Moreover, Chindaprasirt et al. [19] suggest that the NaOH concentration affects the ettringite formation and lowers the strength. However, the single K-activators including KOH and K_2CO_3 exert the lower activation, while the K^+ altogether with Na_2SiO_3 exhibits the highest activation efficiency. It deduces that the

K^+ altogether with $Si(OH)_4$ is beneficial for obtaining a higher mechanical strength of fly-ash-based geopolymer; the detailed reasons are illustrated in the discussion section.

Interestingly, incorporating the 10 wt% SF triggers an obvious enhancement of the mechanical strength as shown in Figure 1. The specimen activated by the mixture of $Na_2SiO_3{\cdot}9H_2O$ and KOH rises to 83.58 MPa (increased by 49%). This means that the activated ≡Si-O-Si≡ chains play a fundamental role in forming a crosslinked network structure, but K^+ presents a rate-determining factor for further improving the strength.

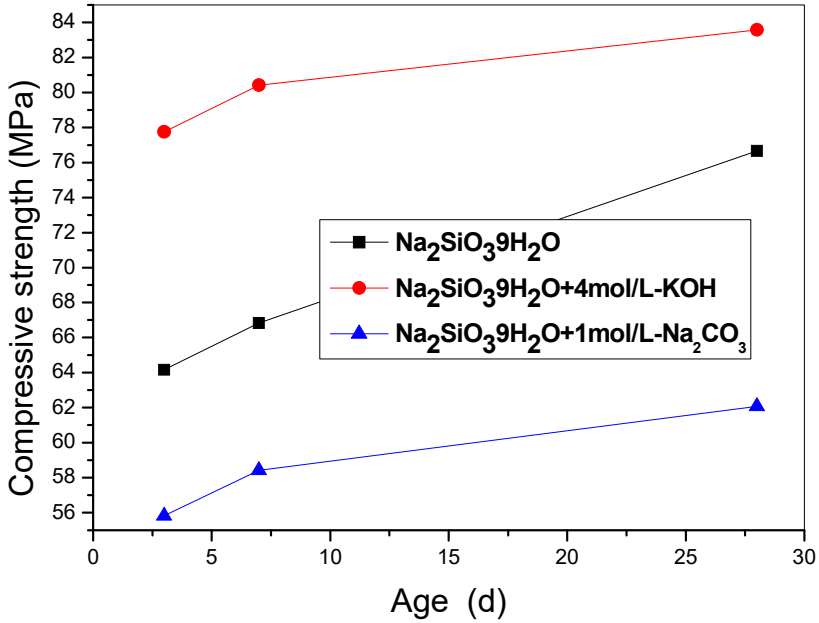


Figure 1. The compressive strength of specimens incorporating SF, including S25~S27.

3.2. Morphology and Microstructure

According to the compressive strength of all specimens, the samples with single KOH, NaOH, and Na_2SiO_3, as well as samples activated by binary activators, are selected to observe their morphology for comparison. Because the study focuses on the effect of different single activators and seeks the optimal activator formulation, the single and binary activators are selected. The morphologies of specimen pastes at 28 days of aging are displayed as a series of SEM images with a magnification of 5000 in Figure 2a–h, and unreacted spherical FA particles decrease and transform into irregularly shaped gels on the fracture surface of pastes, displaying the coexistence of the geopolymeric gels and partially activated FA particles. It is observed that the activation efficiency of the single NaOH is superior to KOH when comparing the Figure 2a with Figure 2b, and more amorphous gels are present on the fracture surface of the NaOH-activated paste.

However, it is worth pointing out that the Na^+ involved in the alkali-activator is prone to forming porous and unevenly distributed framework structures, as shown in Figure 2c, Figure 2f, and Figure 2h, respectively. Meanwhile, activators with K^+ facilitate the formation of plate-type or rod-like structures, as shown in Figures 2d, 2e and 2g, respectively. The uniform and smooth fracture in Figure 2e correspond to the enhanced strength, especially. This indicates that the K^+ favors the condensations or crosslinking between the SiO_4^{4-} and AlO_4^{5-} tetrahedra and boosts the chain propagation of N-(C)-A-S-H amorphous gels, as evidenced by the improved compressive strength. Meanwhile, the porosity of the Na-specimen seems to be on a multiscale in Figure 2f,h; this feature is less pronounced for the K-specimen, as shown in Figure 2e,g, and is in agreement with the Prudhomme [20].

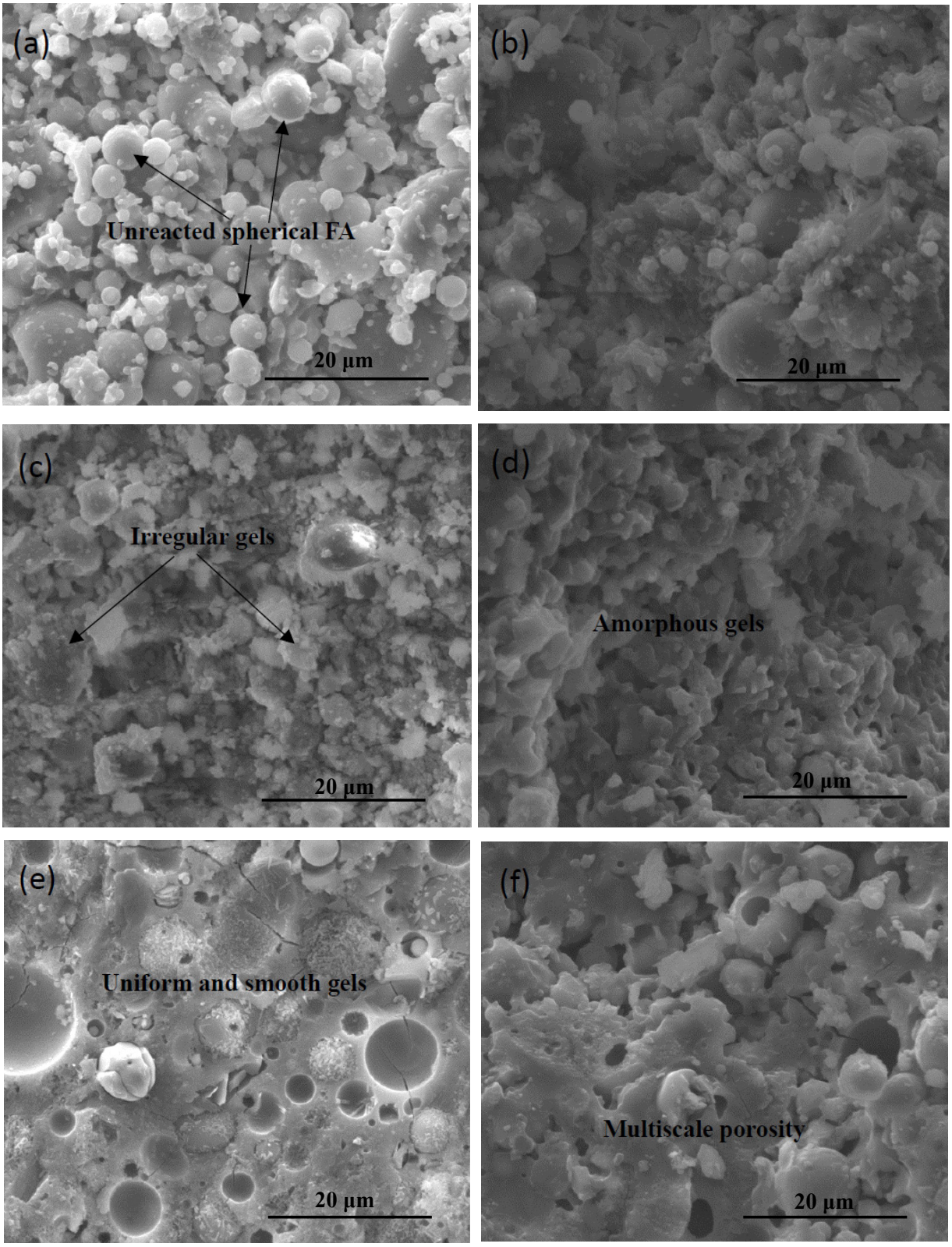


Figure 2. *Cont.*

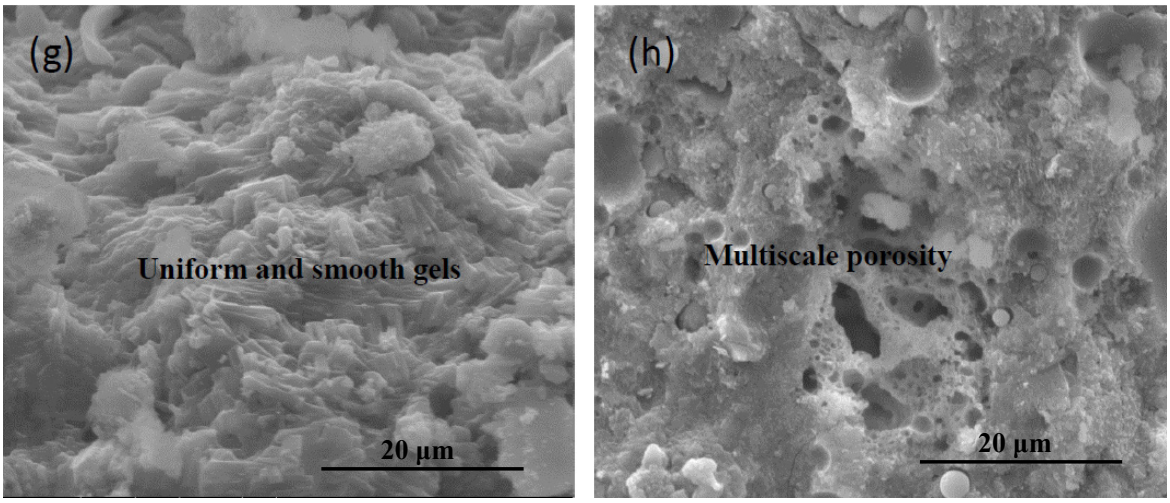


Figure 2. SEM photos of samples with a magnification of 5000×; (**a**) 4 mol/L-KOH, (**b**) 4 mol/L-NaOH, (**c**) 15 wt% Na_2SiO_3, (**d**) 4 mol/L-KOH + 8 mol/L-NaOH, (**e**) 15 wt% Na_2SiO_3 + 4 mol/L-KOH, (**f**) 15 wt% Na_2SiO_3 + 4 mol/L-NaOH, (**g**) 15 wt% Na_2SiO_3 + 1 mol/L-K_2CO_3, and (**h**) 15 wt% Na_2SiO_3 + 1 mol/L-Na_2CO_3.

To further understand the details of the micro-appearance, morphologies of specimens incorporating 10 wt% SF at 28 d aging are displayed in Figure 3; the plate-like or rod-like structures appear on the fracture surface of the specimen with the composite activator of 15 wt% $Na_2SiO_3 \cdot 9H_2O$ and 4 mol/L KOH in comparison to others, while more pores and holes are present on the fracture surface, as in Figure 3a,c. It confirms again that the K^+ boosts the densification process significantly in the Na_2SiO_3-activated fly-ash-based geopolymer.

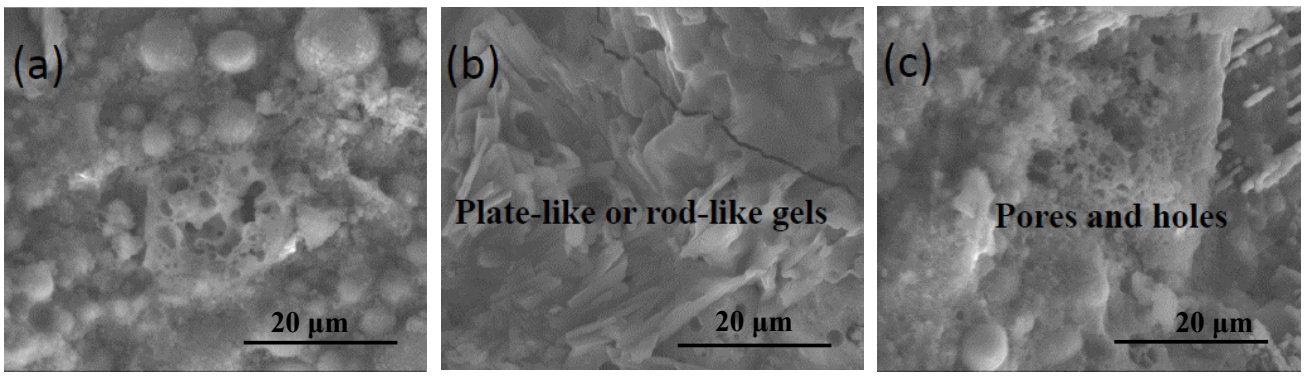


Figure 3. SEM photos of geopolymer incorporated 10 wt% SF with a 5000×. (**a**) 15 wt% Na_2SiO_3, (**b**) 15 wt% Na_2SiO_3 + 4 mol/L-KOH, and (**c**) 15 wt% Na_2SiO_3 + 1 mol/L-Na_2CO_3.

For the sake of exploring the microstructures involved in the specimens with K^+, the pore size distribution of specimens is summarized in Table 3, and it is noted that adding KOH in the composite activators makes the median pore diameter and porosity decline in comparison to the S1. This is because the pore volume with a pore diameter less than 100 nm increases while that with a pore diameter more than 0.2 μm decreases, matching the enhanced mechanical properties. This is because the composite activator (S17, 15 wt% Na_2SiO_3 + 4 mol/L-KOH) facilitates more silicate depolymerization and transforms into siliceous sols, which favors the binder's densification.

Table 3. Pore size distribution of specimens.

Specimens	<100 nm (%)	100–200 nm (%)	>0.2 μm (%)	Median Pore Diameter (nm)	Porosity (%)	Total Intrusion Volume (mL/g)
S1	0.56	14.53	84.91	239.7	23.98	0.1961
S15	27.87	14.18	57.95	104.8	21.36	0.1719
S17	52.54	2.16	45.31	74.6	19.69	0.1578
S25	53.67	6.94	39.39	67.1	19.52	0.1523

S25, the specimen with 10 wt% SF and activated by 15 wt% Na_2SiO_3 + 4 mol/L-KOH.

Meanwhile, the critical pore diameter could be determined as 100 nm according to the tested results; though the well-known critical pore diameter is about 50 nm in porous materials, the geopolymer paste consists of N-(C)-A-S-H chains, C-H-S, and other amorphous silicates. The effective and efficient activation is making the silicon-based sols transform into gels with a pore diameter <100 nm. Furthermore, the threshold diameter of samples by binary activators is determined as 200 nm according to the tested results, due to the pores predominating this range, while the big pore with a pore diameter >200 nm is barely detected.

Analogously, regarding the SF-containing samples, the active silicon-rich sample exerts the smaller pore. The content of the pore diameter <100 nm (critical pore diameter) further climbs to 53.67%, corresponding to the enhanced mechanical property. The median pore diameter further decreases to 67.1 nm from 74.6 nm, because of the pozzolanic effect and filling of SF. Generally, the pore size distribution also provides indirect evidence for the highest activation efficiency of 15 wt% Na_2SiO_3 + 4 mol/L-KOH, especially for the activated silicon-rich system.

3.3. TG/DTG Analysis

The TGA/DTG results of specimens are illustrated in Figure 4. The weight loss and DTG peak temperature of specimen S1, activated only by 15 wt% Na_2SiO_3, are 6.05%, 76.3 °C and 123.5 °C, respectively; specimen S15 with 15 wt% Na_2SiO_3 + 2 mol/L-K_2CO_3 activated is 10.06%, 98.6, and 178.1 °C; specimen S13 activated by 15 wt% Na_2SiO_3 + 2 mol/L-Na_2CO_3 is 10.28%, 92.8, and 175.8 °C; specimen S17 activated by 15 wt% Na_2SiO_3 + 4 mol/L KOH is 8.91%, 71.1, and 182.8 °C; specimen S16 activated by 15 wt% Na_2SiO_3 + 4 mol/L NaOH is 4.51%, 71.5, and 149.7 °C, respectively. The first peak temperature below 100 °C corresponds to the maximum weight loss and is mainly attributed to the free water loss within the geopolymer. Meanwhile, the second peak is mainly attributed to the dehydration of chemical-bonded water within the N-(C)-A-S-H amorphous gels. The S17 exhibits the highest temperature of the second peak, due to the compact and denser structure.

The weight loss mainly derives from the occurrence of dehydration involved in specimens below 300 °C, and the dehydroxylation derived from $Si(OH)_4$ or $[Al(OH)_4]^-$ tetrahedron occurs at about 500 °C [21]. More weight loss implies that more hydroxyls exist within the matrix during the process of alkali-activation. Combined with the results of the pore size distribution, it could be induced that the more volume of small pores, the higher temperature of weight loss. The DTG curves of K-specimens display twists and turns, as shown in Figure 4b,d, meaning that there are more complex and crosslinked structures involved in the specimens compared to the curves of others. It indirectly demonstrates that doping K^+ promotes the formation of the amorphous and network cross-linking of the Na_2SiO_3-activated fly-ash-based geopolymer.

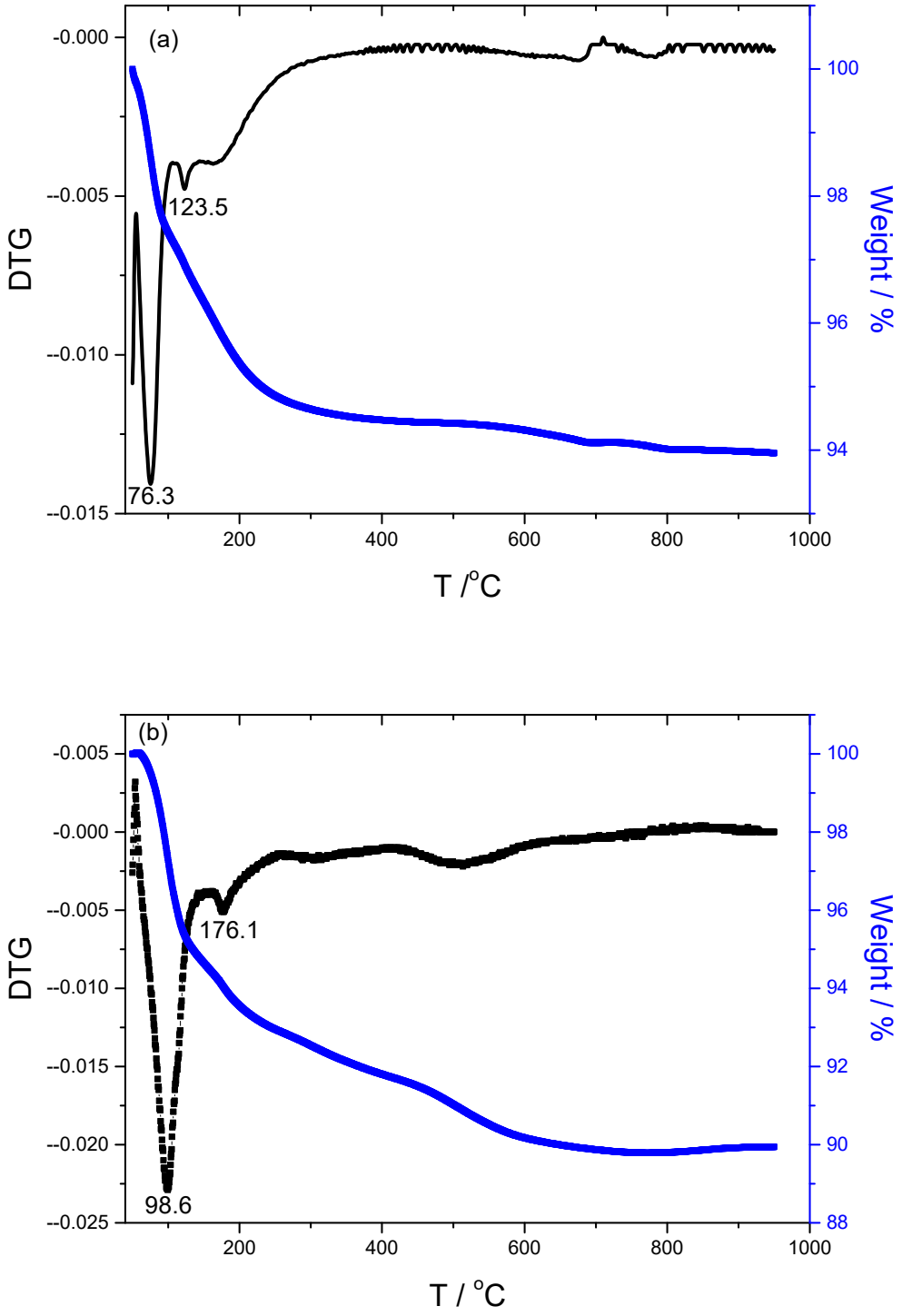
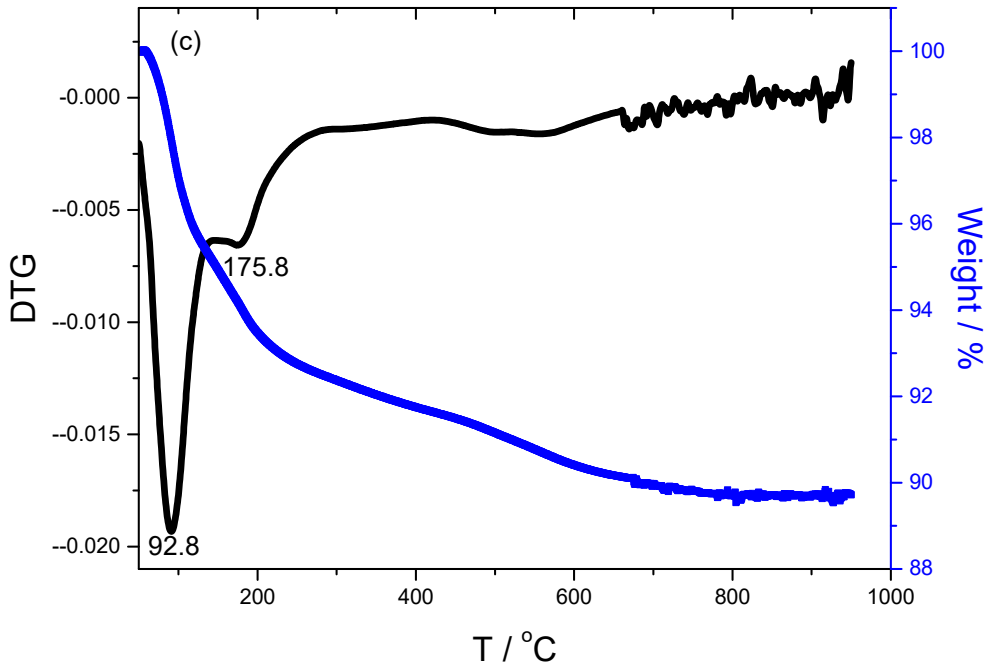


Figure 4. *Cont.*



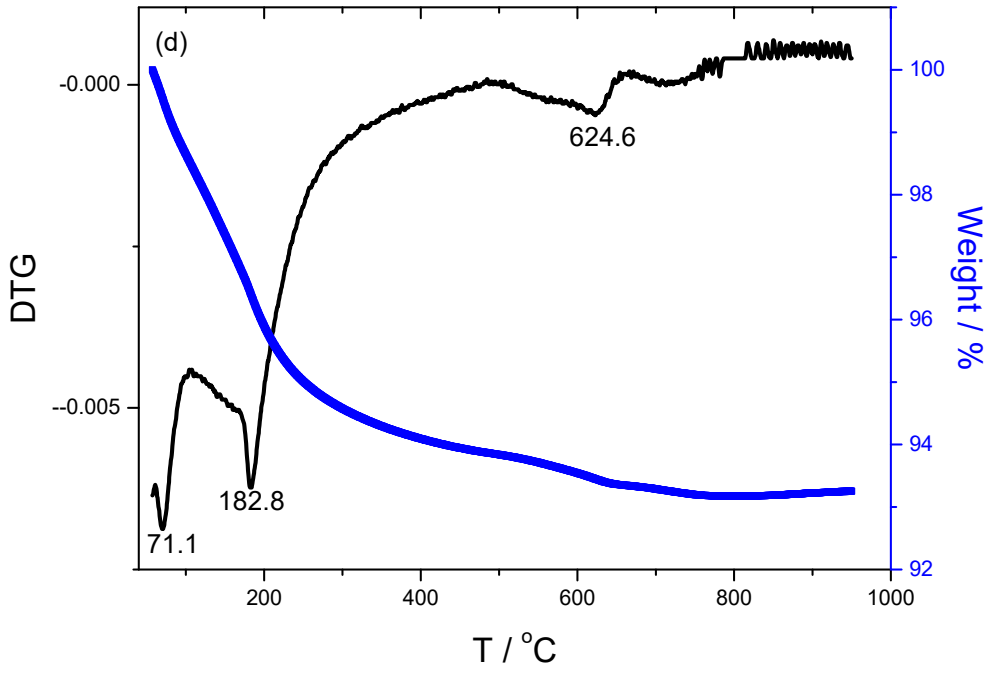


Figure 4. *Cont.*

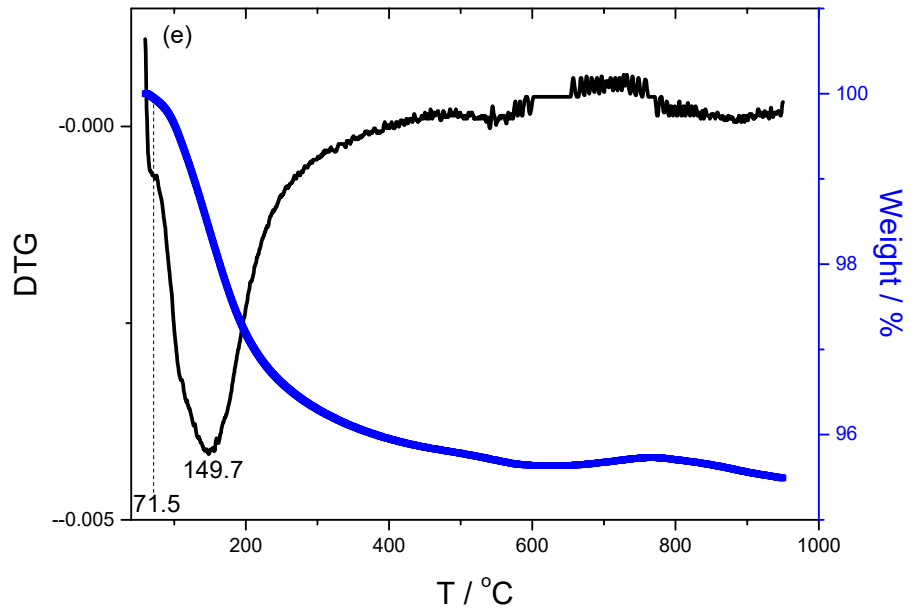


Figure 4. Thermogravimetric analysis of samples including (**a**) S1 activated by 15 wt% Na_2SiO_3, (**b**) S15 activated by 15 wt% Na_2SiO_3 + 2 mol/L-K_2CO_3, (**c**) S13 activated by 15 wt% Na_2SiO_3 + 2 mol/L-Na_2CO_3, (**d**) S17 activated by 15 wt% Na_2SiO_3 + 4 mol/L-KOH, and (**e**) S16 activated by 15 wt% Na_2SiO_3 + 4 mol/L-NaOH, respectively.

3.4. XRD Analysis

There are some peaks derived from the raw fly ash, such as the quartz, mullite, and silimanite, but the peaks, at about 2θ = 27.5, 29.5, 32.3, 24.9, are assigned to the orthoclase [22], as shown in Figure 5. The broad and diffused peaks of about 2θ = 30 are the results of the short-range glassy structures [23]; the increased content of the amorphous silicates means the higher reaction degree of the geopolymerizations corresponds to the enhanced mechanical property. It is obvious that the area between the patterns and the baseline increases after adding SF into the system (Area 2 > Area 1), due to the increased amorphous silicates. Meanwhile, the orthoclase grows and develops with the increasing content of amorphous $Si(OH)_4$, which is in agreement with that increasing the Si/Al ratio in the gels causing the formation of more silicon-rich mineral phases, as orthoclase and sanidine (K [$AlSi_3O_8$]) [24]. Generally, the mineralogical composition is crucial for its properties; especially for the content of amorphous silicates, the higher the amorphous silicates, the higher the compressive strength combined with the mechanical property.

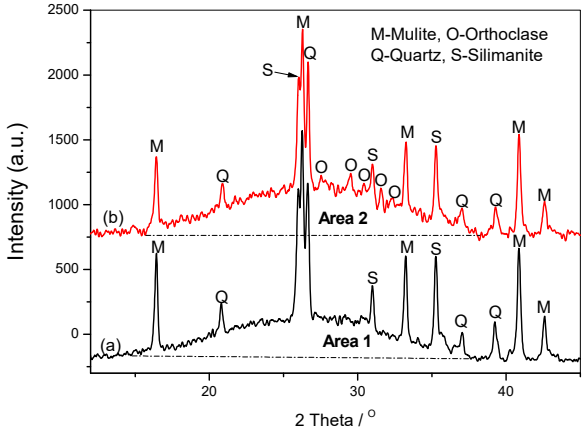


Figure 5. The XRD spectra of samples S17 activated by15 wt% Na_2SiO_3 + 4 mol/L-KOH, including (**a**) sample without SF; (**b**) SF-containing sample.

4. Discussion

Generally, the mechanical strength and microstructure of fly ash geopolymers alkali-activated by binary composite activators are comparatively studied, and the alkaline activators are composed of $Na_2SiO_3 \cdot 9H_2O$, Na_2CO_3, K_2CO_3, NaOH, and KOH. The composite activator of $Na_2SiO_3 \cdot 9H_2O$ + KOH exerts the highest activation efficiency, as evidenced by the enhanced strength and reduced porosity. This is due to the enhanced crosslinking and propagation of N-(C)-A-S-H chains, leading to the increased content of the amorphous silicates (XRD) with uniform and compact morphology (SEM), as well as the improved temperature of the DTG peak.

Essentially, potassium has a smaller hydration sphere than sodium, the OH^- has higher accessibility to Si-O and Al-O bonds in the Na-rich surfaces than K-rich surfaces [25], and the ionic radii proposed for five- and six-coordinate sodium are 1.02 and 1.07 Å, respectively, while the ionic radii for the six- and seven-coordinate K^+ are 1.38 and 1.46 Å, respectively [26]. Therefore, potassium has a weaker affinity to water than sodium [27], exerting the inferior activation efficiency of the single KOH solution to the pure NaOH solution.

However, the composite activator including K^+ and SiO_3^{2-} is crucial to trigger more geopolymerization and forming more amorphous networks, as evidenced by the increased amorphous silicates in XRD patterns. The doped Na_2SiO_3 holds the inherent chain structure ≡Si-O-Si≡ as the silicon-chain precursor, which severs as the "condensation nucleus" to facilitate the further crosslinking and propagation of N-(C)-A-S-H chains. The activated silica tetrahedra derived from doped SF further extend the N-(C)-A-S-H chains, presenting the enhanced area (Area 2 > Area 1) of the amorphous silicates, as shown in XRD patterns. It also verifies that K^+ together with Na_2SiO_3 is beneficial for the formation and growth of siliceous gels [27]. The mixture solution of KOH and Na_2SiO_3 presents a superior performance than that of NaOH and Na_2SiO_3, and the composite activator with 4 M KOH is better than that of 8 M KOH. This is because the excessive alkalinity makes more ions dissolve and precipitate [28], which restrains some alkali metal ions to participate in the propagation of N-(C)-A-S-H chains. The K^+ concentration in the medium is not as pH-dependent as Na^+ [29].

Secondly, water and potassium transform into interconnected networks through hydrogen bonding, and the K^+-H_2O hydrogen-bonded network holds a stabilizing effect [24]. Meanwhile, the Na^+ could not convert into the hydrogen-bonded networks. It means that more widespread K^+ exists in the system, providing the sustained catalysis for the polycondensations among N-(C)-A-S-H chains, due to the K^+ contributing a higher disorder degree or crosslinking for the K-based system [30]. Furthermore, Cioffi et al. [31] also suggest that the larger size of potassium has a favorable effect on cross-linking even if the polycondensation degree left is unchanged, which is beneficial for the distortion, transformation, and cross-linking, leading to an increased endothermic peak (DTG) and compact morphology (SEM).

Thirdly, due to the lower viscosity of the KOH solution in comparison with NaOH [32], it also plays a critical role in geopolymerications involved in the system containing sufficient activated $Si(OH)_4$, leading to enhanced mechanical strength, while a higher NaOH concentration solution causes aluminosilicate gel precipitation at a very early stage.

Furthermore, the SF-containing specimen also proves this point. The increased activated silicon-chain precursor provides the beneficial conditions for K^+ to form more cross-linked N-(C)-A-S-H chains, leading to an obvious increase in strength. It is consistent with the reports of Kathirvel et al. [33,34] that silicate in the activator powder reacts with calcium to produce more volume of the C-A-S-H gel. However, our finding confirms that the K^+ predominantly controls the step of reorganization in fly-ash-based geopolymerical systems, according to the process of "depolymerization-reorganization". The evolution process of K^+ in the alkali-activated fly ash system is affected not only by the activator (e.g., composition) but also by the concentration (e.g., 4 M and 8 M).

Consequently, the depolymerizations of silicates occur and form some $Si(OH)_4$ and $[Al(OH)_4]^-$ monomers under a stronger alkali condition, but the in-situ crosslinked ≡Si-O-Si≡

chains as the "condensation nucleus" provide the preconditions of the subsequent polycondensations or propagation of N-(C)-A-S-H. The K^+ in the composite activators boosts the reorganization or restructuring of activated alumina and silica, and the as-formed amorphous sols could fill the pores and holes corresponding to enhanced strength, leading to an increase in the pore volume of the diameter less than 100 nm, as well as an increase in weight loss temperatures of specimens from TG/DTG results.

5. Conclusions

The comparative study on the microstructure of the fly-ash-based geopolymer, activated by the binary composite activator, is investigated by characterization techniques, which consists of $Na_2SiO_3 \cdot 9H_2O$, Na_2CO_3, K_2CO_3, NaOH, and KOH with various concentrations. The composite activator of $Na_2SiO_3 \cdot 9H_2O$ + KOH exerts the highest activation efficiency evidenced by the enhanced strength, proposing the synergy activation between the inherent ≡Si-O-Si≡ chain precursor derived from Na_2SiO_3 and K^+'s catalysis. It reveals that K^+ plays a crucial role in geopolymerations with the prerequisites of some inherent ≡Si-O-Si≡ chains as the "condensation nucleus", boosting the crosslinking and propagation of N-(C)-A-S-H chains. The as-formed amorphous siliceous sols also could fill the pores or holes and present a compact morphology, leading to an increase in the pore volume of the diameter less than 100 nm, as well as an increase in weight loss temperatures from TG/DTG results. It explores an efficient and cost-effective preparation of fly-ash-based geopolymer for developing solid waste recycling techniques.

Author Contributions: J.Z., funding acquisition, resources, and writing—review and editing. Y.W., conceptualization, writing—review and editing, formal analysis, methodology, data curation, project administration, visualization, and funding acquisition. All authors have read and agreed to the published version of the manuscript.

Funding: This work is supported by the Natural Science Foundation of Shaanxi Province (2022JM-222), Social Science Foundation of Shaanxi Province (2022R046), the open fund from Key Laboratory of Solid Waste Treatment and Resource Recycling, Ministry of Education, Southwest University of Science and Technology (22kfgk02).

Data Availability Statement: Not applicable.

Acknowledgments: This work is supported by the Natural Science Foundation of Shaanxi Province (2022JM-222), Social Science Foundation of Shaanxi Province (2022R046), the open fund from Key Laboratory of Solid Waste Treatment and Resource Recycling, Ministry of Education, Southwest University of Science and Technology (22kfgk02).

Conflicts of Interest: The authors declare no conflict of interest.

References

1. Deventer, J.; Provis, J.; Duxson, P.; Lukey, G. Reaction mechanisms in the geopolymeric conversion of inorganic waste to useful products. *J. Hazard. Mater.* **2007**, *139*, 506–513. [CrossRef] [PubMed]
2. Fernández-Jiménez, A.; Palomo, A.; Criado, M. Microstructure development of alkali-activated fly ash cement: A descriptive model. *Cem. Concr. Res.* **2005**, *35*, 1204–1209. [CrossRef]
3. Wang, S.; Liu, B.; Zhang, Q.; Wen, Q.; Lu, X.; Xiao, K.; Ekberg, C.; Zhang, S. Application of geopolymers for treatment of industrial solid waste containing heavy metals: State-of-the-art review. *J. Clean. Prod.* **2023**, *390*, 136053. [CrossRef]
4. Peng, X.; Li, H.; Hu, Y. Preparation of metakaolin-fly ash cenosphere based geopolymer matrices for passive fire protection. *J. Mater. Res. Technol.* **2023**, *23*, 604–610. [CrossRef]
5. Harmal, A.; Khouchani, O.; El-Korchi, T.; Tao, M.; Walker, H.W. Bioinspired brick-and-mortar geopolymer composites with ultra-high toughness. *Cem. Concr. Compos.* **2023**, *137*, 104944. [CrossRef]
6. Pławecka, K.; Bazan, P.; Lin, W.-T.; Korniejenko, K.; Sitarz, M.; Nykiel, M. Development of Geopolymers Based on Fly Ashes from Different Combustion Processes. *Polymers* **2022**, *14*, 1954. [CrossRef]
7. Sarıdemir, M.; Çelikten, S. Effects of Ms modulus, Na concentration and fly ash content on properties of vapour-cured geopolymer mortars exposed to high temperatures. *Constr. Build. Mater.* **2023**, *363*, 129868. [CrossRef]
8. Komljenović, M.; Baščarević, Z.; Bradić, V. Mechanical and microstructural properties of alkali-activated fly ash geopolymers. *J. Hazard. Mater.* **2010**, *181*, 35–42. [CrossRef]

9. Cheng, T.-W.; Chiu, J.P. Fire-resistant geopolymer produced by granulated blast furnace slag. *Miner. Eng.* **2003**, *16*, 205–210. [CrossRef]
10. Tchakouté, H.K.; Rüscher, C.H.; Kong, S.; Kamseu, E.; Leonelli, C. Geopolymer binders from metakaolin using sodium water glass from waste glass and rice husk ash as alternative activators: A comparative study. *Constr. Build. Mater.* **2016**, *114*, 276–289. [CrossRef]
11. Esaifan, M.; Khoury, H.; Aldabsheh, I.; Rahier, H.; Hourani, M.; Wastiels, J. Hydrated lime/potassium carbonate as alkaline activating mixture to produce kaolinitic clay based inorganic polymer. *Appl. Clay Sci.* **2016**, *126*, 278–286. [CrossRef]
12. Wang, W.; Fan, C.; Wang, B.; Zhang, X.; Liu, Z. Workability, rheology, and geopolymerization of fly ash geopolymer: Role of alkali content, modulus, and water–binder ratio. *Constr. Build. Mater.* **2023**, *367*, 130357. [CrossRef]
13. Yan, S.; Pan, D.; Dan, J.; Wang, J.; Yu, Y. Calcium carbide residue and Glauber's salt as composite activators for fly ash-based geopolymer. *Cem. Concr. Compos.* **2023**, *140*, 105081. [CrossRef]
14. Yang, J.; Bai, H.; He, X.; Zeng, J.; Su, Y.; Wang, X.; Zhao, H.; Mao, C. Performances and microstructure of one-part fly ash geopolymer activated by calcium carbide slag and sodium metasilicate powder. *Constr. Build. Mater.* **2023**, *367*, 130303. [CrossRef]
15. Wang, H.; Zhao, X.; Gao, H.; Yuan, T.; Zhang, X. The effects of salt-loss soda residue and oxalate acid on property and structure of fly ash-based geopolymer. *Constr. Build. Mater.* **2023**, *366*, 130214. [CrossRef]
16. Yliniemi, J.; Nugteren, H.; Illikainen, M.; Tiainen, M.; Weststrate, R.; Niinimäki, J. Lightweight aggregates produced by granulation of peat-wood fly ash with alkali activator. *Int. J. Miner. Process.* **2016**, *149*, 42–49. [CrossRef]
17. Görhan, G.; Kürklü, G. The influence of the NaOH solution on the properties of the fly ash-based geopolymer mortar cured at different temperatures. *Compos. Part B* **2014**, *58*, 371–377. [CrossRef]
18. Somna, K.; Jaturapitakkul, C.; Kajitvichyanukul, P.; Chindaprasirt, P. NaOH-activated ground fly ash geopolymer cured at ambient temperature. *Fuel* **2011**, *90*, 2118–2124. [CrossRef]
19. Chindaprasirt, P.; Thaiwitcharoen, S.; Kaewpirom, S.; Rattanasak, U. Controlling ettringite formation in FBC fly ash geopolymer concrete. *Cem. Concr. Compos.* **2013**, *41*, 24–28. [CrossRef]
20. Prudhomme, E.; Michaud, P.; Joussein, E.; Clacens, J.-M.; Rossignol, S. Role of alkaline cations and water content on geomaterial foams: Monitoring during formation. *J. Non-Crystalline Solids* **2011**, *357*, 1270–1278. [CrossRef]
21. Guerrieri, M.; Sanjayan, J.G. Behavior of combined fly ash/slag-based geopolymers when exposed to high temperatures. *Fire Mater.* **2010**, *34*, 163–175. [CrossRef]
22. Kürklü, G. The effect of high temperature on the design of blast furnace slag and coarse fly ash-based geopolymer mortar. *Compos. Part B* **2016**, *92*, 9–18. [CrossRef]
23. Vassilev, S.V.; Baxter, D.; Vassileva, C.G. An overview of the behaviour of biomass during combustion: Part I. Phase-mineral transformations of organic and inorganic matter. *Fuel* **2013**, *112*, 391–449. [CrossRef]
24. MarieSkofteland, B.; Ellesad, O.; Lillerud, K. Potassium merlinoite: Crystallization, structural and thermal properties. *Microporous Mesoporous Mater.* **2001**, *43*, 61–71. [CrossRef]
25. Lee, W.; Deventer, J. Structural reorganisation of class F fly ash in alkaline silicate solutions. Colloids and Surfaces A: Physicochem. *Eng. Asp.* **2002**, *211*, 49–66. [CrossRef]
26. Skorina, T. Ion exchange in amorphous alkali-activated aluminosilicates: Potassium based geopolymers. *Appl. Clay Sci.* **2014**, *87*, 205–211. [CrossRef]
27. Wang, Y.; Zhao, J. Comparative study on flame retardancy of silica fume-based geopolymer activated by different activators. *J. Alloys Compd.* **2018**, *743*, 108–114. [CrossRef]
28. Yang, J.; Zhang, Q.; He, X.; Su, Y.; Zeng, J.; Xiong, L.; Zeng, L.; Yu, X.; Tan, H. Low-carbon wet-ground fly ash geopolymer activated by single calcium carbide slag. *Constr. Build. Mater.* **2022**, *353*, 129084. [CrossRef]
29. Murri, A.N.; Medri, V.; Ruffini, A.; Papa, E.; Landi, E. Study of the chemical activation of hydroxyapatite rich ashes as raw materials for geopolymers. *Ceram. Int.* **2015**, *41*, 9734–9744. [CrossRef]
30. Peng, Z.; Vance, K.; Dakhane, A.; Marzke, R.; Neithalath, N. Microstructural and ^{29}Si MAS NMR spectroscopic evaluations of alkali cationic effects on fly ash activation. *Cem. Concr. Compos.* **2015**, *57*, 34–43. [CrossRef]
31. Cioffi, R.; Maffucci, L.; Santoro, L. Optimization of geopolymer synthesis by calcination and polycondensation of a kaolinitic residue. *Resour. Conserv. Recycl.* **2003**, *40*, 27–38. [CrossRef]
32. Hwang, C.-L.; Huynh, T.-P. Effect of alkali-activator and rice husk ash content on strength development of fly ash and residual rice husk ash-based geopolymers. *Constr. Build. Mater.* **2015**, *101*, 1–9. [CrossRef]
33. Rajan, H.S.; Kathirvel, P. Sustainable development of geopolymer binder using sodium silicate synthesized from agricultural waste. *J. Clean. Prod.* **2021**, *286*, 124959. [CrossRef]
34. Nassar, A.K.; Kathirvel, P. Effective utilization of agricultural waste in synthesizing activator for sustainable geopolymer technology. *Constr. Build. Mater.* **2023**, *362*, 129681. [CrossRef]

Disclaimer/Publisher's Note: The statements, opinions and data contained in all publications are solely those of the individual author(s) and contributor(s) and not of MDPI and/or the editor(s). MDPI and/or the editor(s) disclaim responsibility for any injury to people or property resulting from any ideas, methods, instructions or products referred to in the content.